Amorphous Calcium Carbonate

International Edition: DOI: 10.1002/anie.201603176
German Edition: DOI: 10.1002/ange.201603176

Water as the Key to Proto-Aragonite Amorphous $CaCO_3$

*Masoud Farhadi-Khouzani, Daniel M. Chevrier, Peng Zhang, Niklas Hedin, and Denis Gebauer**

Abstract: *Temperature and pH value can affect the short-range order of proto-structured and additive-free amorphous calcium carbonates (ACCs). Whereas a distinct change occurs in proto-vaterite (pv) ACC above 45 °C at pH 9.80, proto-calcite (pc) ACC (pH 8.75) is unaffected within the investigated range of temperatures (7–65 °C). IR and NMR spectroscopic studies together with EXAFS analysis showed that the temperature-induced change is related to the formation of proto-aragonite (pa) ACC. The data strongly suggest that the binding of water molecules induces dipole moments across the carbonate ions in pa-ACC as in aragonite, where the dipole moments are due to the symmetry of the crystal structure. Altogether, a (pseudo-)phase diagram of the $CaCO_3$ polyamorphism in which water plays a key role can be formulated based on variables of state, such as the temperature, and solution parameters, such as the pH value.*

Amorphous calcium carbonate (ACC) plays an important role as an intermediate in $CaCO_3$ biomineralization processes,[1] and can be used as the inorganic component in biocompatible hybrids.[2] Investigations of the structures of both biogenic and synthetic ACCs and their correlation with thermodynamic stability and polymorph selection in crystallization and biomineralization have recently received significant attention.[3] Water can be a structural constituent of ACC, and plays a pivotal role for its kinetic and thermodynamic stability.[4] Accordingly, associated water molecules can govern the transformation of ACCs into crystalline phases;[5] however, their role in the proposed ACC (pseudo-)polyamorphism remains unclear.[1b] While the water content of ACC can vary,[5,6] there are indications for a prevalence of stoichiometric $CaCO_3{\cdot}H_2O$.[1b,4b,7] High pressures can lead to short-range aragonite-like structures,[8] and in aqueous systems, the formation of proto-calcite (pc) and proto-vaterite (pv) ACC can be controlled by adjusting the pH value.[3a] Finally, the formation of ACC under aqueous conditions via prenucleation clusters and nanoscopic liquid–liquid demixing indeed points to the importance of water for the precursors and intermediates of $CaCO_3$.[4a,9]

Herein, we investigated the effect of temperature on the structure and composition of ACC at two pH levels, namely pH 8.75 and 9.80, owing to their relevance for the formation of pc- and pv-ACC, respectively. Our data strongly suggest that structural water is fundamental to the formation of proto-aragonite (pa) ACC above 50 °C at pH 9.80.

Aragonite is preferably formed at elevated temperatures,[10] although this phase becomes thermodynamically stable at much higher temperatures than those that are typically accessible by aqueous routes at ambient pressures.[11] The robust formation of pure-phase aragonite under kinetic control occurs at both investigated pH levels above approximately 45 °C (Section S3-1 and Figures S1–S3 in the Supporting Information). To elucidate the potential role of ACC proto structures in this context, pc- and pv-ACC (at pH 8.75 and 9.80, respectively) were synthesized at 7 °C and at temperatures between 25 °C and 65 °C with increments of 10 °C by using an ethanol quench. The obtained ACC phases consist of spherical nanoparticles with diameters of 15–20 nm (Figure 1 a for pH 9.80 and 65 °C). Neither the temperature nor the pH value strongly affect their size (Figure S4). The selected area electron diffraction (SAED) patterns of all samples display diffuse rings, underpinning their amorphous character (insets in Figure 1 a and Figure S4). Interestingly, a distinct change occurred in pv-ACC at temperatures of 45 °C and 55 °C (Figure 1 b), which is prominent in the carbonate ν_1 IR spectral region. This effect arguably suddenly occurs between 45–50 °C (Figure S5). Notably, as opposed to calcite and vaterite, the carbonate ν_1 vibrational mode is IR-allowed in the anhydrous polymorph aragonite because of its symmetry (space group *Pmcn*; point group $2/m2/m2/m$), causing a dipole moment within the plane of the flat and triangular carbonate ions. The increase in intensity in the carbonate ν_1 spectral region is thus in agreement with pa-ACC. The very broad band suggests that structural water plays a role in causing this effect. However, the absence of any temperature-induced transition in pc-ACC at pH 8.75 also indicates that the carbonate environments present in pv-ACC are essential for the formation of pa-ACC (Section S3-2, Figures S5 and S6, and Table S1). In fact, pa-ACC yields aragonite in a solid-state transformation upon heating to 500 °C, or by slow crystallization in aqueous ethanolic environments at room temperature, whereas this is not the case for pv-ACC (Section S3-3 and Figures S7–S13). Thus pa-ACC likely is the intermediate relevant for aragonite formation, which was successfully isolated and transferred into the solid state.

Thermogravimetric analysis (TGA) indicates that calcium hydroxide co-precipitated alongside ACC in all experiments.

[*] M. Farhadi-Khouzani, Dr. D. Gebauer
Department of Chemistry, Physical Chemistry
University of Konstanz
Universitätsstrasse 10, Box 714, 78457 Konstanz (Germany)
E-mail: denis.gebauer@uni-konstanz.de
D. M. Chevrier, Prof. Dr. P. Zhang
Department of Chemistry & School of Biomedical Engineering
Dalhousie University, Halifax (Canada)
Prof. Dr. N. Hedin
Department of Materials and Environmental Chemistry
Stockholm University
10691 Stockholm (Sweden)

Supporting information for this article can be found under: http://dx.doi.org/10.1002/anie.201603176.

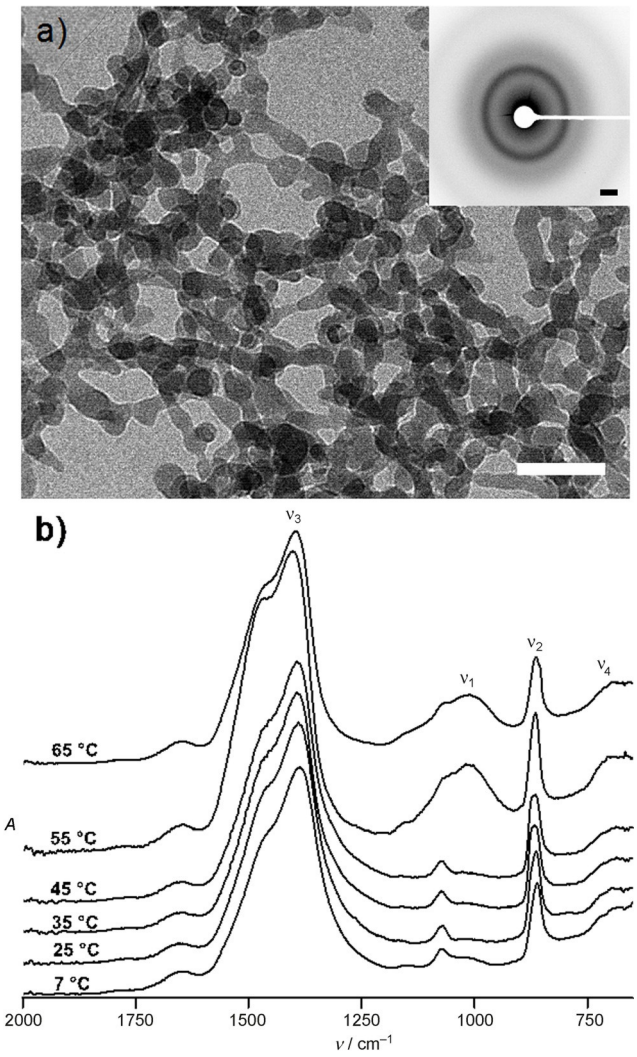

Figure 1. a) TEM image and SAED pattern (inset) of pa-ACC synthesized at 65 °C and pH 9.80. The SAED pattern is shown as the negative to make weak features clearer. Scale bars: 100 nm and 2 nm^{-1} for TEM and SAED, respectively. b) ATR/FTIR spectra of ACCs at different temperatures (pH 9.80); the spectra are shown staggered for the sake of clarity.

This side product is formed by the quench in ethanol rather than being an actual solution species (Section S3-4, Figures S15–S17, and Table S3). Consistently, IR and solid-state NMR spectroscopic data (Section S3-4) suggest that the calcium hydroxide constitutes a distinct phase. Owing to the higher temperatures that are used for quenching pa-ACC (pH 9.80, >50 °C), the hydroxide content reaches approximately (40 ± 5) wt% (Table S3). Nevertheless, the formation of crystalline $Ca(OH)_2$ was not apparent from the ATR/FTIR spectra, as there was no sharp band at 3643 cm^{-1} (Figure S5).[12] Closer inspection of the IR spectra (Figure 1b; see also Figure S5 and Table S2) furthermore reveals that the carbonate ν_1 band of pv-ACC is superimposed on the broad feature assigned to pa-ACC. Taken together, these findings show that the sample contains at least three distinct environments, namely 1) pv-ACC, 2) pa-ACC, and 3) (amorphous) calcium hydroxide.

As opposed to pc- and pv-ACC (see Ref. [3a] and Figure S18), the ^{13}C magic angle spinning (MAS) NMR spectrum of the sample containing pa-ACC showed clear deviations from a single Gaussian line (Figure 2a; signal-to-noise ratio (S/N) $\approx$ 20). The S/N ratio could not be improved

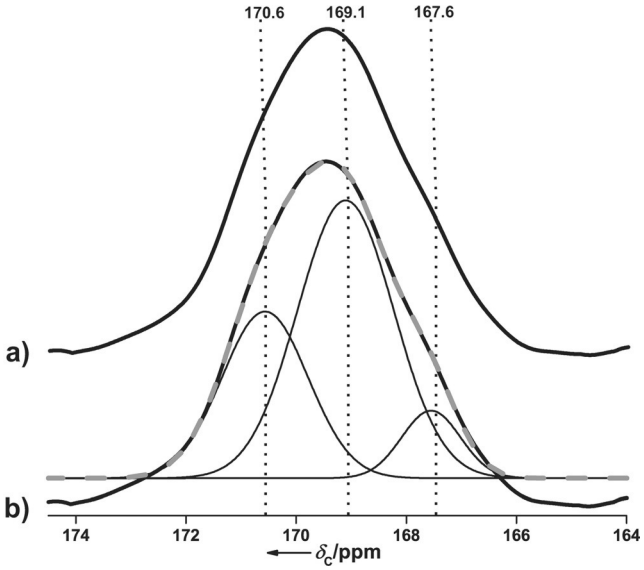

Figure 2. ^{13}C magic-angle-spinning NMR spectra of the sample containing pa-ACC (pH 9.80, 65 °C). Vertical dotted lines are a guide for the eye. a) Spectrum recorded by single pulses (bold black trace). b) Deconvolution of the spectrum into three Gaussians (thin black lines). The dashed gray line represents the sum of the respective Gaussians to illustrate the agreement of the deconvolution with the experimental data. Please see the main text for a discussion of the robustness of the deconvolution.

significantly by any reasonable experimental effort (Sections S1-1 and S2-4), precluding the acquisition of reliable ^{1}H$\rightarrow^{13}$C cross-polarization spectra (data not shown), or even heteronuclear correlation experiments. Although the S/N ratio is satisfactory for quantitative analysis,[13] the overlap of distinct resonances at the given peak widths does impair the robustness of any deconvolution. Given the results obtained by IR spectroscopy and TGA, deconvolution is justifiable even though the as-obtained quantitative information will be associated with distinct errors. The NMR spectrum can be deconvoluted into three Gaussian-shaped spectral contributions, whereas the maximum of the dominating resonance is located at $\delta=169.1$ ppm (Figure 2b). This corresponds to a pv-ACC environment (Tables S1 and S4), identified independently through the superimposed band in the IR spectrum (see above). A second resonance is centered at $\delta=170.6$ ppm, which is consistent with an aragonite-like proto structure (the single resonance of aragonite is found at $\delta=170.5$ ppm; Table S1), in accordance with the IR spectroscopy results. The relative abundance of these distinct environments is approximately 1:2 (Table S4), that is, a larger amount of pv-ACC coexists with pa-ACC in this sample. A third chemical environment is characterized by a Gaussian spectral contribution centered at $\delta=167.6$ ppm. This is in agreement with an ACC form that contains hydroxide[14] (or ikaite, although the

occurrence of ikaite-like environments at high temperatures is unexpected; see Table S1). Considering the S/N ratio, this minor spectral contribution may also be due to a misinterpretation of noise. In any case, hydroxides lead to the effective shielding of neighboring carbonates because of their additional charge ($\delta = 167.6$ ppm),[14] suggesting that the hydroxide content in the pa-ACC environment, which is the most deshielded one, is not significant ($\delta = 170.6$ ppm; Figure 2b).

Analysis of the Fourier-transformed Ca K-edge extended X-ray absorption fine structure (EXAFS; Section S2-5, Figure S19, and Table S5) yields a value of 2.41 Å for the first shell distance (Ca–O), which is higher than those for pc-ACC (2.36 Å) and pv-ACC (2.39 Å). A corresponding trend was found for calcite (2.34 Å), vaterite (2.37 Å), and aragonite (2.47 Å). Taking into account that the Ca–O distance of the sample is a weighted average of short-range-ordered structures of approximately 30% pa-ACC and 60% pv-ACC (based on NMR analysis; see Table S4), the Ca–O distance in pa-ACC is the longest of all proto-structured ACCs. Furthermore, the average EXAFS-derived Ca–O coordination number of 3.7 ± 1.1 for the sample containing pa-ACC is somewhat larger than for pv- and pc-ACC (ca. 2), but still lower than for calcite and vaterite (6) as well as aragonite (9; Table S5).

In conclusion, pa-ACC is formed at pH 9.80 above 45 °C. Global rationalization of our results is possible considering structural water molecules associated with carbonate ions. These water molecules can induce dipole moments across the carbonate ions, leading to the effect observed in the IR spectra. Second, this dipole moment can displace electrons from the central carbon atom, leading to the deshielded environment of pa-ACC as observed by NMR spectroscopy. Third, binding between water and carbonate can explain the increase in the average Ca–O distances determined by EXAFS, which may be accompanied by a somewhat closer packing (as in aragonite). The confirmation of this collection of indirect evidence was possible by a closer inspection of the IR spectra for the temperature-induced crystallization of pa-ACC in comparison to pv-ACC (Section S3-3 and Figures S7 and S9): The IR spectral features of water remain significantly more prominent in pa-ACC with increasing temperature than in pv-ACC, and it remains a structural constituent up to 400 °C. The broad and strong carbonate ν_1 band only disappears with the remaining water upon complete crystallization at 500 °C.

Aragonite is formed at both pH values above approximately 45 °C, whereas a significant amount of pa-ACC can be found only at pH 9.80. It could be speculated that low amounts of pa-ACC are present at both pH values, which grow faster because of the directing role of dipole–dipole interactions in aggregation-based pathways,[6a] thereby facilitating robust kinetic aragonite formation. In additive-controlled scenarios, organic–inorganic interactions could lead to similar effects that may be relevant to selective aragonite formation in biomineralization.

Experimental Section

For details, see the Supporting Information, Sections S1 and S2. In brief, calcium chloride solutions were added to carbonate buffers of pH 8.75 and pH 9.80 at different temperatures, while the pH was maintained at a constant level by automatic titration. Before nucleation, the $CaCO_3$ precursors were quenched with an excess of ethanol, then washed, and isolated.

Acknowledgements

D.G. is a Research Fellow of the Zukunftskolleg of the University of Konstanz and supported by the Fonds der Chemischen Industrie. N.H. thanks the Swedish Energy Agency for support, and the Swedish Research Council and the Knut and Alice Wallenberg Foundation for NMR equipment grants. D.M.C. is supported by an NSERC CGS Alexander Graham Bell scholarship. P.Z. acknowledges support from NSERC Canada. The CLS@APS (Sector 20-BM) facilities at the APS are supported by the U.S. DOE, Basic Energy Sciences, NSERC Canada, the University of Washington, the CLS, and the APS. Use of the APS was supported by the U.S. DOE (DEAC02-06CH11357). Technical assistance was provided by Dr. Robert Gordon and Dr. Zou Finfrock.

Keywords: amorphous calcium carbonate · biomineralization · NMR spectroscopy · polyamorphism · water

How to cite: *Angew. Chem. Int. Ed.* **2016**, *55*, 8117–8120
Angew. Chem. **2016**, *128*, 8249–8252

[1] a) L. Addadi, S. Raz, S. Weiner, *Adv. Mater.* **2003**, *15*, 959–970; b) J. H. E. Cartwright, A. G. Checa, J. D. Gale, D. Gebauer, C. I. Sainz-Díaz, *Angew. Chem. Int. Ed.* **2012**, *51*, 11960–11970; *Angew. Chem.* **2012**, *124*, 12126–12137; c) Y. Politi, T. Arad, E. Klein, S. Weiner, L. Addadi, *Science* **2004**, *306*, 1161–1164.

[2] a) T. Y. Cheang, S. M. Wang, Z. J. Hu, Z. H. Xing, G. Q. Chang, C. Yao, Y. Liu, H. Zhang, A. W. Xu, *J. Mater. Chem.* **2010**, *20*, 8050–8055; b) J. H. Wei, T. Cheang, B. Tang, H. M. Xia, Z. H. Xing, Z. H. Chen, Y. Fang, W. Chen, A. W. Xu, S. M. Wang, J. H. Luo, *Biomaterials* **2013**, *34*, 1246–1254; c) D. Gebauer, V. Oliynyk, M. Salajkova, J. Sort, Q. Zhou, L. Bergström, G. Salazar-Alvarez, *Nanoscale* **2011**, *3*, 3563–3566; d) Y. Zhao, Z. Luo, M. H. Li, Q. Y. Qu, X. Ma, S. H. Yu, Y. L. Zhao, *Angew. Chem. Int. Ed.* **2015**, *54*, 919–922; *Angew. Chem.* **2015**, *127*, 933–936; e) E. Tolba, W. E. G. Müller, B. M. Abd El-Hady, M. Neufurth, F. Wurm, S. Wang, H. C. Schröder, X. Wang, *J. Mater. Chem. B* **2016**, *4*, 376–386.

[3] a) D. Gebauer, P. N. Gunawidjaja, J. Y. P. Ko, Z. Bacsik, B. Aziz, L. J. Liu, Y. F. Hu, L. Bergström, C. W. Tai, T. K. Sham, M. Edén, N. Hedin, *Angew. Chem. Int. Ed.* **2010**, *49*, 8889–8891; *Angew. Chem.* **2010**, *122*, 9073–9075; b) R. S. K. Lam, J. M. Charnock, A. Lennie, F. C. Meldrum, *CrystEngComm* **2007**, *9*, 1226–1236; c) S. Raz, P. C. Hamilton, F. H. Wilt, S. Weiner, L. Addadi, *Adv. Funct. Mater.* **2003**, *13*, 480–486; d) J. Rieger, M. Kellermeier, L. Nicoleau, *Angew. Chem. Int. Ed.* **2014**, *53*, 12380–12396; *Angew. Chem.* **2014**, *126*, 12586–12603; e) D. Zahn, *ChemPhysChem* **2015**, *16*, 2069–2075.

[4] a) P. Raiteri, J. D. Gale, *J. Am. Chem. Soc.* **2010**, *132*, 17623–17634; b) M. F. Khouzani, D. M. Chevrier, P. Güttlein, K. Hauser, P. Zhang, N. Hedin, D. Gebauer, *CrystEngComm* **2015**, *17*, 4842–4849.

[5] a) J. Ihli, W. C. Wong, E. H. Noel, Y. Y. Kim, A. N. Kulak, H. K. Christenson, M. J. Duer, F. C. Meldrum, *Nat. Commun.* **2014**, *5*, 3169; b) A. V. Radha, A. Navrotsky, *Cryst. Growth Des.* **2015**, *15*, 70 – 78.
[6] a) C. Rodriguez-Navarro, K. Kudlacz, O. Cizer, E. Ruiz-Agudo, *CrystEngComm* **2015**, *17*, 58 – 72; b) F. M. Michel, J. MacDonald, J. Feng, B. L. Phillips, L. Ehm, C. Tarabrella, J. B. Parise, R. J. Reeder, *Chem. Mater.* **2008**, *20*, 4720 – 4728.
[7] R. Innocenti Malini, Y. G. Bushuev, S. A. Hall, C. L. Freeman, P. M. Rodger, J. H. Harding, *CrystEngComm* **2016**, *18*, 92 – 101.
[8] A. Fernandez-Martinez, B. Kalkan, S. M. Clark, G. A. Waychunas, *Angew. Chem. Int. Ed.* **2013**, *52*, 8354 – 8357; *Angew. Chem.* **2013**, *125*, 8512 – 8515.
[9] a) D. Gebauer, M. Kellermeier, J. D. Gale, L. Bergström, H. Cölfen, *Chem. Soc. Rev.* **2014**, *43*, 2348 – 2371; b) A. F. Wallace, L. O. Hedges, A. Fernandez-Martinez, P. Raiteri, J. D. Gale, G. A. Waychunas, S. Whitelam, J. F. Banfield, J. J. De Yoreo, *Science* **2013**, *341*, 885 – 889.
[10] J. Kawano, N. Shimobayashi, A. Miyake, M. Kitamura, *J. Phys. Condens. Matter* **2009**, *21*, 425102.
[11] J. C. Jamieson, *J. Chem. Phys.* **1953**, *21*, 1385 – 1390.
[12] V. C. Farmer, *The Infrared Spectra of Minerals*, Mineralogical Society, London, **1974**.
[13] Y. L. Martin, *J. Magn. Reson. Ser. A* **1994**, *111*, 1 – 10.
[14] a) H. Nebel, M. Neumann, C. Mayer, M. Epple, *Inorg. Chem.* **2008**, *47*, 7874 – 7879; b) A. L. Goodwin, F. M. Michel, B. L. Phillips, D. A. Keen, M. T. Dove, R. J. Reeder, *Chem. Mater.* **2010**, *22*, 3197 – 3205.

Received: March 31, 2016
Published online: June 2, 2016

